

The Weibel instability in a circular rarefaction wave

M.E. Dieckmann¹, K. Quinn², G Sarri², L Romagnani³, GC Murphy⁴, I Kourakis²,
A. Macchi⁵, J. Fuchs³, O. Willi⁶, M Borghesi²

¹ Dept of Science and Technology, Linköping University, Norrköping, Sweden

² Centre for Plasma Physics, Queen's University Belfast, Belfast, U.K.

³ LULI, Ecole Polytechnique, CNRS, CEA, UPMC, Palaiseau, France

⁴ Dublin Institute for Advanced Studies, Dublin, Ireland

⁵ CNR, Istituto Nazionale di Ottica, Pisa, Italy

⁶ Univ. Düsseldorf, Inst. Laser & Plasmaphys., Düsseldorf, Germany

Abstract: Instabilities behind the front of a cylindrically expanding plasma have been investigated experimentally and with a particle-in-cell simulation. Tubelike filamentary structures form behind the front of a plasma created by irradiating wire targets with a ps-duration and intense ($\sim 10^{19}$ W cm⁻²) laser pulse. These filaments exhibit coherent magnetic fields with a remarkable stability ($\geq 10^3 \omega_p^{-1} \omega_p$: plasma frequency). PIC simulations indicate that an instability driven by a thermal anisotropy of the electron population is the cause. This instability requires a plasma density gradient and hot electrons. It can thus contribute to the generation of strong sustained magnetic fields in astrophysical jets.

The experiment:

The experimental setup, which is used to sample the magnetic field distribution in the laser-generated plasma, is described in Fig. 1. A sequence of radiochromic film (RCF) images have been taken to follow the time evolution of the expanding plasma. Figure 2 shows RCF images [1], which describe the interaction between the probing protons and the field distribution of the expanding plasma. The laser impact took place in the wire's center. The plasma expansion is approximately cylindrical between this point and the wire's end points. The central vertical structure corresponds to the strong **B**-field driven by the current of the hot electrons expanding along the wire's surface.

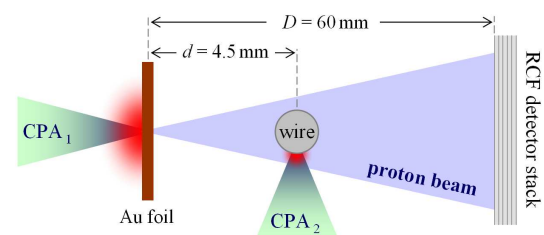


Figure 1: The laser pulse CPA2 heats up the wire target. Ions are radially accelerated by the surface electric field that is generated by the escape of fast electrons. The laser pulse CPA1 interacts with a gold foil and accelerates by the same (TNSA) process surface (probing) protons. The RCF detector stack records the angular and energy distribution of the probing protons, which provides information about the magnetic field distribution.

The magnetic field distribution is initially uniform along the wire's axis (See Fig. 2(a)). Thin stable horizontal structures are visible at the later times in Figs. 2(b,c), which are oriented orthogonally to the wire's axis. These structures correspond to magnetic fields, which enwrap current filaments that point in the radial direction. Their late formation shows that these structures are not directly generated by the laser pulse. The lower image in Fig. 2 shows the model distribution of current filaments, on which we have based our particle tracing studies. Particle tracing can reproduce the RCF images if we set the peak magnetic field to $|\mathbf{B}|_{max} \approx 15$ T and the spacing between the filaments to $40\mu\text{m}$.

The simulation:

The expansion of the exploding wire sufficiently far from the laser impact point and from the wire's endpoints is cylindrical (See Fig. 2(a)). The plasma expansion can be approximated by that in a cross-section of the wire. The initial conditions for our particle-in-cell (PIC) simulation [2] with periodic boundary conditions, are shown in Fig. 3.

The temperature of the electrons is 32 keV and that of the protons is 10 eV. We use the correct mass ratio between both species. Both species have uniform and equal number densities in the cloud. The cloud is surrounded by vacuum and initially the electromagnetic fields are set to zero in the box. The high thermal speed of the electrons implies that some leave the cloud, which results in a negative net charge outside of the cloud and a positive excess charge inside it. The resulting ambipolar electric field points in the radial direction and accelerates the ions. A radially expanding rarefaction wave develops, which is initially azimuthally symmetric. In what follows, we discuss the plasma state at the time $t\omega_p = 550$. We exploit the azimuthal symmetry of the rarefaction wave and integrate the electron distribution accordingly.

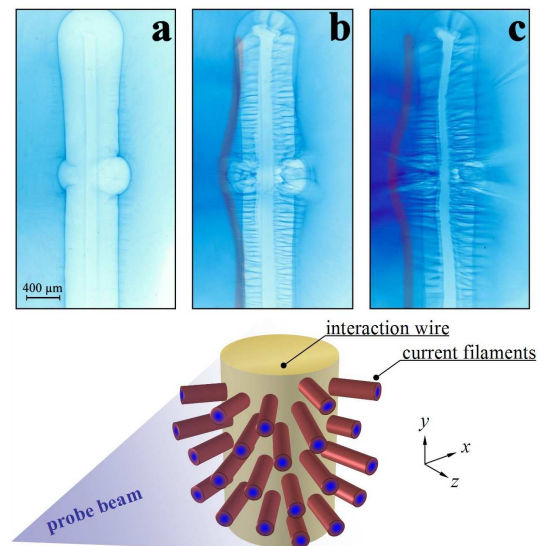


Figure 2: Upper image: Snapshots of the magnetic field distribution at the times 10ps (A), 30ps (B) and 50ps (C). Lower image: Distribution of the current filaments that reproduces the RCF images.

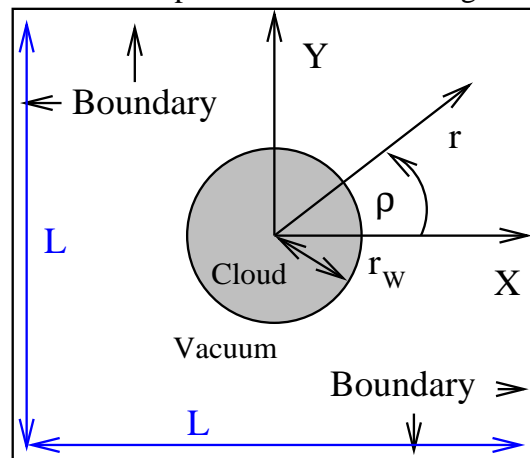


Figure 3: The initial plasma distribution in our 2D PIC simulation.

Figure 4 shows the azimuthally averaged 10-logarithmic electron and proton phase space density distributions, normalized to their respective peak values. Initially their density is uniform within the plasma cloud. The plasma density close to the initial cloud boundary has decreased. The protons close to the cloud perimeter have been accelerated and their motion away from the cloud has resulted in a reduction of their density. Quasi-neutrality implies a similar electron density evolution. The mean speed of the proton distribution increases with the distance from the cloud perimeter and the density decreases.

The ions are accelerated by the ambipolar electric field, which is shown in Fig. 5(a). Its modulus is proportional to the plasma density gradient. It peaks at the proton front (See Fig. 4(b)). The non-zero electric field within the initial cloud perimeter (overplotted black circle) evidences the plasma erosion close to the original boundary. The growth of magnetic fields close to the initial cloud boundary are observed. The growth of the in-plane magnetic field in Fig. 5(b) by the secondary instability discussed in Ref. [2] is related to a disalignment of the plasma density gradient and the electric field. This disalignment arises from the superposition of the electric field component, which is induced by the out-of-plane magnetic field, and the density gradient-driven ambipolar electric field. The origin of the out-of-plane magnetic field observed in Fig. 5(c) is revealed by Fig. 6.

Figure 6 shows the azimuthally averaged electron number density $n_e(r)$, the effective plasma frequency $\omega_p(r) \propto (n_e(r))^{1/2}$, the thermal anisotropy $A(r)$ and the azimuthally integrated total magnetic energy density $E_B(r)$. The thermal anisotropy is defined as the ratio between the

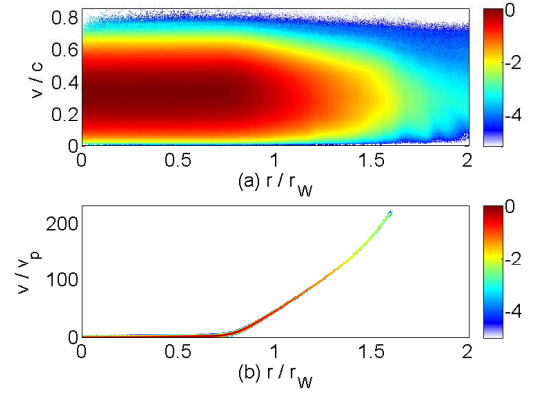


Figure 4: The azimuthally integrated phase space density distributions of the electrons (a) and protons (b).

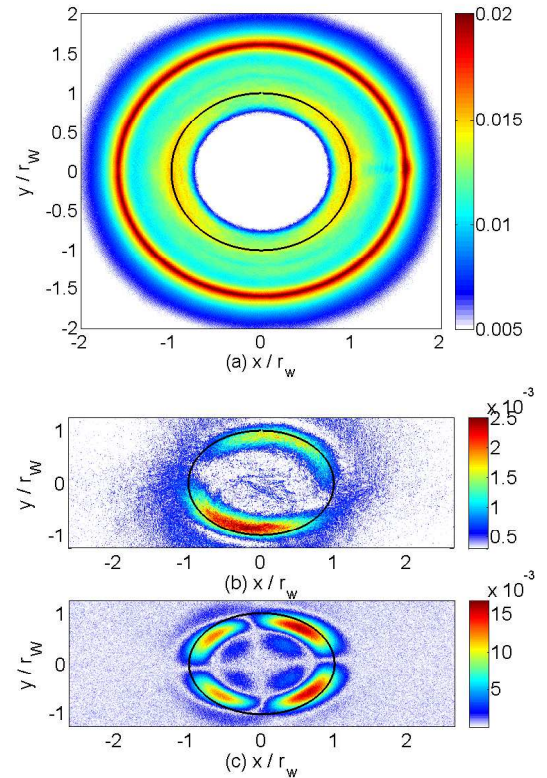


Figure 5: Panel (a) shows the electric field modulus. Panels (b) and (c) show the in-plane magnetic field modulus and the out-of-plane magnetic field modulus.

electron thermal energy density in the radial direction and that in the azimuthal direction.

A value $A < 1$ implies that the electrons have lost more energy in the radial than in the azimuthal direction. This energy loss is linked by their slowdown in the ambipolar electric field in Fig. 5(a). The thermal anisotropy gives rise to an instability similar to that described by Weibel [3]. The instability observed in the rarefaction wave grows fastest where A is small and ω_p is still large.

Summary:

We have observed experimentally the growth of magnetic fields in the rarefaction wave triggered by the laser-ablation of a wire. We have modeled this expansion with a particle-in-cell simulation. The simulation has revealed that the likely cause of the magnetic field growth is a thermal anisotropy-driven Weibel instability. This instability has previously been observed in planar rarefaction waves [4]. Its growth is thus robust against changes in the rarefaction wave geometry. The instability is driven by the slowdown of hot electrons in the ambipolar electric field of a density gradient. Such plasma conditions are likely to exist in energetic astrophysical jets, like in those that drive gamma-ray bursts, and the gradient-driven Weibel instability may thus contribute to their observed magnetization.

Acknowledgments: This work was supported by Vetenskapsrådet (DNR 2010-4063), EP-SRC (EP/E035728/1, EP/C003586/1, EP/D043808/1), Consejería de Educación y Ciencia (ENE2009-09276), the Junta de Comunidades de Castilla-La Mancha (PAI08-0182-3162), SFI (08/RFP/PHY1694). Computer time and support was provided by the HPC2N in Umeå and by the ICHEC in Dublin.

References

- [1] K. Quinn et al., *Phys. Rev. Lett.* **108** (2012) 135001
- [2] M.E. Dieckmann et al., *New J. Phys.* **14** (2012) 023007
- [3] E.S. Weibel, *Phys. Rev. Lett.* **2** (1959) 83
- [4] C. Thauray et al., *Phys. Rev. E* **82** (2010) 016408

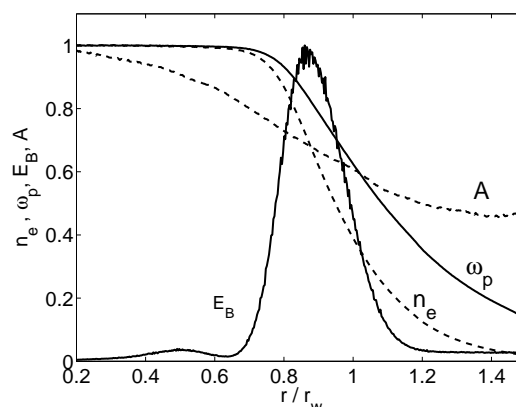


Figure 6: The radially averaged electron density $n_e(r)$, $\omega_p(r) \propto (n_e(r))^{1/2}$, the ratio A between the electron thermal energies in the radial and azimuthal directions and the azimuthally integrated magnetic energy density $E_B(r)$.